Impacts of the Leading Modes of Tropical Indian Ocean Sea Surface Temperature Anomaly on Sub-Seasonal Evolution of the Circulation and Rainfall over East Asia during Boreal Spring and Summer

Senfeng LIU[1,2] and Anmin DUAN[1,2,3*]

1 *State Key Laboratory of Numerical Modelling for Atmospheric Sciences and Geophysical Fluid Dynamics, Institute of Atmospheric Physics, Chinese Academy of Sciences, Beijing* 100029
2 *College of Earth Science, University of Chinese Academy of Sciences, Beijing* 100049
3 *Collaborative Innovation Center on Forecast and Evaluation of Meteorological Disasters, Nanjing University of Information Science & Technology, Nanjing* 210044

(Received June 13, 2016; in final form August 13, 2016)

ABSTRACT

The two leading modes of the interannual variability of the tropical Indian Ocean (TIO) sea surface temperature (SST) anomaly are the Indian Ocean basin mode (IOBM) and the Indian Ocean dipole mode (IODM) from March to August. In this paper, the relationship between the TIO SST anomaly and the sub-seasonal evolution of the circulation and rainfall over East Asia during boreal spring and summer is investigated by using correlation analysis and composite analysis based on multi-source observation data from 1979 to 2013, together with numerical simulations from an atmospheric general circulation model. The results indicate that the impacts of the IOBM on the circulation and rainfall over East Asia vary remarkably from spring to summer. The anomalous anticyclone over the tropical Northwest Pacific induced by the warm IOBM is closely linked with the Pacific–Japan or East Asia–Pacific teleconnection pattern, which persists from March to August. In the upper troposphere over East Asia, the warm phase of the IOBM generates a significant anticyclonic response from March to May. In June and July, however, the circulation response is characterized by enhanced subtropical westerly flow. A distinct anomalous cyclone is found in August. Overall, the IOBM can exert significant influence on the western North Pacific subtropical high, the South Asian high, and the East Asian jet, which collectively modulate the precipitation anomaly over East Asia. In contrast, the effects of the IODM on the climate anomaly over East Asia are relatively weak in boreal spring and summer. Therefore, studying the impacts of the TIO SST anomaly on the climate anomaly in East Asia should take full account of the different sub-seasonal response during boreal spring and summer.

Key words: East Asia, sub-seasonal evolution, Indian Ocean basin mode, Indian Ocean dipole mode

Citation: Liu, S. F., and A. M. Duan, 2017: Impacts of the leading modes of tropical Indian Ocean sea surface temperature anomaly on sub-seasonal evolution of the circulation and rainfall over East Asia during boreal spring and summer. *J. Meteor. Res.*, **31**(1), 171–186, doi: 10.1007/s13351-016-6093-z.

1. Introduction

The tropical Indian Ocean (TIO) sea surface temperature (SST) anomaly and its climatic effects have received extensive research attention (Li et al., 2001; Yang et al., 2010; Xie et al., 2016). The Indian Ocean basin mode (IOBM) is the dominant pattern of SST anomaly interannual variability over the TIO. It peaks in late boreal winter or early spring and persists to summer in the following year of El Niño events. The IOBM primarily arises from the influence of ENSO over the equatorial tropical Pacific on the TIO (Klein et al., 1999; Xie et al., 2016). The second leading mode of the TIO is the Indian Ocean dipole mode (IODM), with the different sign of the SST anomaly between the east and the west of the TIO, which develops and matures in boreal summer and autumn, then disappears rapidly after peaking in October (Saji et al., 1999; Webster et al., 1999; Li and Mu, 2001;

Supported by the National Natural Science Foundation of China (91337216), Chinese Academy of Sciences Project (XDA11010402), China Meteorological Administration Special Public Welfare Research Fund (GYHY201406001), and Special Program for Applied Research on Super Computation of the NSFC–Guangdong Joint Fund (the second phase).

*Corresponding author: amduan@lasg.iap.ac.cn.

Yang et al., 2015).

Previous studies have indicated that a warm IOBM can induce an enhancement of the western North Pacific subtropical high and the South Asian high (Wu et al., 2000; Terao and Kubota, 2005; Yang et al., 2007; Yang and Liu, 2008; He et al., 2015). Wu et al. (2000) proposed a two-stage mechanism of thermal adaption whereby an in-situ anomalous cyclone in the low-level troposphere, induced by the warm SST anomaly in the TIO, can enhance southerlies and promote deep convective precipitation to its east, which results in anomalous anticyclonic circulation over the tropical Northwest Pacific and South Asia. Yang et al. (2007) considered the IOBM as a capacitor, prolonging the influences of ENSO through the effects of charging and discharging, such as a strengthened South Asian high and an anomalous anticyclone over the tropical Northwest Pacific. The warm TIO SST with deep convection generates a baroclinic Kelvin wave into the western Pacific and induces suppressed convection and an anomalous anticyclone over the tropical Northwest Pacific (Xie at al., 2009; Wu et al., 2009). Lu and Lu (2015) demonstrated an asymmetric relationship between the TIO SST and the western North Pacific summer climate. A series of numerical simulations verified the conclusion that a warm TIO can result in a tropical Northwest Pacific anomalous anticyclone (Wu and Liu, 1995; Li et al., 2008; Huang et al., 2010; Wu et al., 2010; Chowdary et al., 2011; Hu and Duan, 2015). A positive feedback mechanism based on the Indo–western Pacific Ocean capacitor effect explains the inter-basin interaction between the tropical Northwest Pacific anomalous anticyclone and the North Indian Ocean warming and answers the question as to why the IOBM can last to summer (Du et al., 2009; Kosaka et al., 2013).

As for the region of East Asia, the anomalous anticyclone associated with the suppressed convection over the tropical Northwest Pacific affects the East Asian climate to the north via the Pacific–Japan (PJ) pattern or East Asia–Pacific (EAP) pattern (Nitta, 1987; Huang and Sun, 1992; Lau et al., 2000; Wang et al., 2001; Kim et al., 2009). Kosaka et al. (2013) investigated the coupling between the North Indian Ocean and the PJ pattern, suggesting that the PJ pattern impacts the Indian Ocean through a westward propagating atmospheric Rossby wave; and in return, SST in the TIO feeds back to the PJ pattern via a tropospheric Kelvin wave. A warm IOBM may impact the East Asian climate via modulating the local Hadley cell, leading to suppressed convection over the Maritime Continent and a positive rainfall anomaly over southern China (Wu et al., 2009; Zhu et al., 2014). Moreover, the IOBM induces a new atmospheric heating source in South Asia, which can excite circumglobal teleconnection in the boreal Northern Hemisphere midlatitude atmosphere in summer (Ding and Wang, 2005; Yang et al., 2009). Based on numerical experiments from an atmospheric general circulation model (AGCM), Wu and Liu (1995) argued that the SST anomaly over the equatorial tropical Pacific has no direct impact on the East Asian climate, while the TIO warming is a crucial factor of influence—a result also obtained in other studies (Yang et al., 2007; Wu et al., 2009; Hu and Duan, 2015).

Studies have also documented the impacts of the IODM on global climate (Li and Mu, 2001; Guan et al., 2003; Saji and Yamagata, 2003), and the teleconnections of the IOD can cause anomalies in the East Asian summer climate (Guan and Yamagata, 2003). Yuan et al. (2008) investigated the influence of the IOD on the Asian summer monsoon in the following year. Yang et al. (2010) found that the IOBM in spring has a much stronger linkage with the Asian summer monsoon, while the IODM in fall shows a stronger relationship with the Asian winter monsoon.

The interannual variability of climate in East Asia is closely related to the livelihoods of billions of people, as well as the economic development of many countries, including China, South Korea, and Japan. Previous studies have focused mainly on the seasonal-mean relationship between the TIO SST and East Asian climate anomalies, rather than the sub-seasonal evolution. The aim of the present study, therefore, is to investigate the impacts of the TIO SST anomaly on the sub-seasonal evolution of the circulation and rainfall in East Asia during boreal spring and summer on the interannual timescale. Specifically, we seek to address the following questions through data diagnosis and the results of numerical experiments: (1) What are the different impacts of the TIO SST anomaly on the climate anomaly in different months during spring and summer? (2) How does the TIO SST anomaly modulate the circulation systems and rainfall anomaly in East Asia? (3) Which mode plays the more effective role—the IOBM or IODM?

Following this introduction, Section 2 introduces the data and the AGCM used in the study. Section 3 presents the data diagnosis results concerning the IOBM, the IODM, and their effects. Section 4 sets out possible explanations for the IOBM and IODM impacts, based on the results of numerical experiments. Finally, conclusions are given in Section 5.

2. Data and model

2.1 *Data*

Monthly mean datasets used in this study include: SST data from the Hadley Centre (HadISST1; 1° × 1°) (Rayner et al., 2003); three-dimensional reanalysis data from the ECMWF (ERA-Interim; 1° × 1°; 37 pressure levels; variables consisting of geopotential height, temperature, zonal and meridional components of horizontal wind, and vertical velocity, in the isobaric coordinate system) (Dee et al., 2011); and precipitation data from version 2.1 of the Global Precipitation Climatology Project (2.5° × 2.5°) (Adler et al., 2003) and the Asian Precipitation Highly-Resolved Observational Data Integration Towards Evaluation of Water Resource (APHRODITE; 0.25° × 0.25°) (Yatagai et al., 2009). The time range of all the data used in this study is from 1979 to 2013, except APHRODITE, which is only available from 1979 to 2007. In order to focus on the interannual variability, long-term linear trends in all data are removed.

2.2 *AGCM*

The AGCM employed in the present study is F/SAMIL, which stands for the Finite-volume/Spectral Atmospheric Model developed by the IAP/LASG (Institute of Atmospheric Physics/State Key Laboratory of Numerical Modeling for Atmospheric Sciences and Geophysical Fluid Dynamics) (Zhou et al., 2012, 2015; Yu et al., 2014). F/SAMIL has two dynamical core versions—FAMIL and SAMIL. We choose the FAMIL version with a finite-volume dynamical core at the resolution of C48 (1.875° × 1.875°; about 200 km) and 32 vertical levels, whose top level is 2.16 hPa. The physical parameterizations of this model are consistent with the description in Hu and Duan (2015).

3. Observed relationship between the TIO SST anomaly and climatic anomaly

3.1 *Leading modes of TIO SST sub-seasonal evolution from March to August*

The TIO SST anomalies over the region (30°S–30°N, 30°–105°E) from March to August are analyzed by using the empirical orthogonal function (EOF) method. Then, the first and second leading modes are derived for each month.

The EOF results of the TIO SST anomaly (Fig. 1) show that the first leading EOF mode (EOF1) and the second leading EOF mode (EOF2) are the IOBM and IODM, from March to August. In terms of explained variations, the EOF1s account for 45.1%, 43.0%, 39.2%, 37.9%, 32.0%, and 28.8%, respectively; and the EOF2s account for 12.4%, 13.0%, 15.1%, 11.0%, 13.9%, and 16.0%. This means that the EOF1s and EOF2s contribute to most of the variation in the TIO SST interannual variability. There are, however, some differences among the different months in terms of the EOF spatial patterns. From March to August, the maximum SST anomaly centers of the IOBM migrate gradually northwestward from the tropical southern Indian Ocean to the Arabian Sea. As for the IODM, the spatial structure is characterized by a positive maximum center in the southwestern Indian Ocean and a negative maximum center in the southeastern Indian Ocean. Particularly, the SST anomaly in the Arabian Sea is positive in spring and turns negative in summer.

The IOBM and IODM indexes of the six months are defined by the time coefficient series of the corresponding principal component, respectively, which show obvious interannual variation. All the pairwise cross-correla-

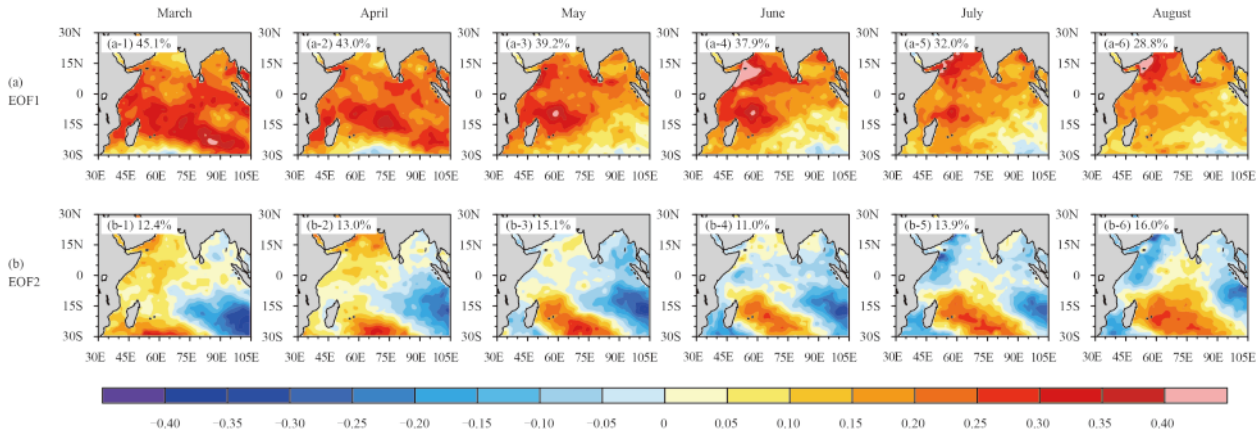

Fig. 1. Spatial patterns of (a) EOF1 and (b) EOF2 of the SST anomaly in the tropical Indian Ocean from March to August. The explained variance is marked in the top-left corner of each panel.

tion coefficients between the IOBM indexes of the six months are greater than 0.6, passing the 95% confidence level (Fig. 2a), and those between the IODM indexes are above 0.3, mostly passing the 95% confidence level (Fig. 2b). This implies that the IOBM and IODM persist steadily from spring to summer, despite the IODM's persistence being relatively weaker than the IOBM's.

To demonstrate the relationship between the interannual variability of the East Asian summer monsoon (EASM) and that of the SST anomaly, an EASM index is defined by the difference in the anomalous zonal wind over the region (22.5°–32.5°N, 110°–140°E) and the region (5°–15°N, 90°–130°E) in summer (Wang et al., 2008). This can reflect the leading pattern of EASM interannual variability and can be calculated conveniently; and its positive anomaly is identical to the main enhanced rainfall belt from the Yangtze River to Japan in summer. The correlation coefficients between the EASM index and IOBM index from March to August are 0.435, 0.431, 0.504, 0.613, 0.512, and 0.474, respectively, passing the 95% confidence level. However, the correlation coefficients between the EASM index and IODM index from March to August are –0.079, –0.126, –0.096, –0.036, –0.125, and –0.144, failing to pass the significance test. Therefore, the IOBM is remarkably associated with the EASM from March to August, but the IODM is not. The correlation maps between the EASM index and the global SST anomaly from March to August also confirm that the IOBM is likely to be the most stable and persistent SST anomaly impacting the interannual variability of the EASM (figures omitted here).

3.2 *Sub-seasonal relationship between East Asian climate and the IOBM*

Composite analysis is used to reveal the linkages of the IOBM with the displacement of the South Asian high, the western North Pacific subtropical high, the East Asian jet, and the East Asian main rainfall belt. Tables 1 and 2 show the typical warm and cold years of the IOBM, selected according to whether the IOBM index is above (or below) 0.8 (–0.8) standard deviations. It is clear that most of the warm IOBM years follow El Niño events, while only about half of the cold IOBM years follow La Niña events. Besides, most of the warm IOBM events can persist longer than cold events.

Simultaneous correlation maps are used to illustrate the relationship between the IOBM and the circulation/precipitation. In the tropical region, a warm IOBM is linked with a significant positive anomalous geopotential height at 200 hPa from the TIO to the western Pacific (Fig. 3a). Along with geopotential height increasing in the upper troposphere, the South Asian high establishing from June is affected remarkably by the IOBM in summer (June–July–August). The composite analysis shows that the South Asian high tends to enhance and expand to the south, east, and west with the IOBM warming in comparison with cooling in summer (Fig. 4). Its ridge line moves southward more obviously in June than that in July and August. Under the condition of a warm IOBM, the eastern part of the South Asian high over East Asia is stronger in July than that in June and August, which is consistent with the characteristics in the climatology.

Over the TIO, a warm IOBM is closely related to a

Table 1. Warm IOBM years in the composite analysis

Month	Year	Number
March	1983, 1987, 1988, 1998, 2005, 2010	6
April	1983, 1987, 1988, 1991, 1998, 2003, 2010	7
May	1983, 1987, 1991, 1998, 2010	5
June	1983, 1987, 1991, 1998, 2003, 2007, 2010	7
July	1983, 1987, 1988, 1998, 2003, 2009, 2010	7
August	1983, 1987, 1988, 1998, 2009, 2012	6

Table 2. Cold IOBM years in the composite analysis

Month	Year	Number
March	1982, 1986, 1989, 2000, 2008	5
April	1982, 1986, 1989, 2000, 2008, 2011	6
May	1984, 1985, 1989, 1996, 1999, 2000, 2004, 2008, 2013	9
June	1984, 1985, 1989, 1994, 2000, 2004, 2013	7
July	1981, 1984, 1985, 1989, 1994, 1996, 2000, 2004	8
August	1981, 1984, 1985, 1986, 1989, 1994, 1996, 2013	8

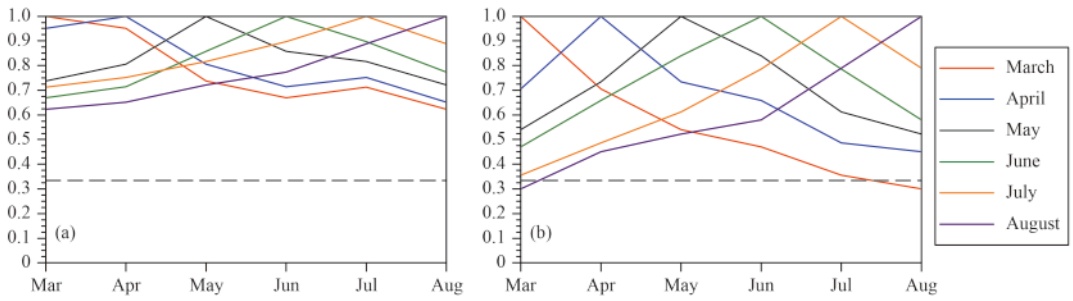

Fig. 2. Pairwise cross-correlation coefficients between the indexes of the (a) Indian Ocean basin mode and (b) the Indian Ocean dipole mode, from March to August. The horizontal dashed lines denote the 95% confidence level.

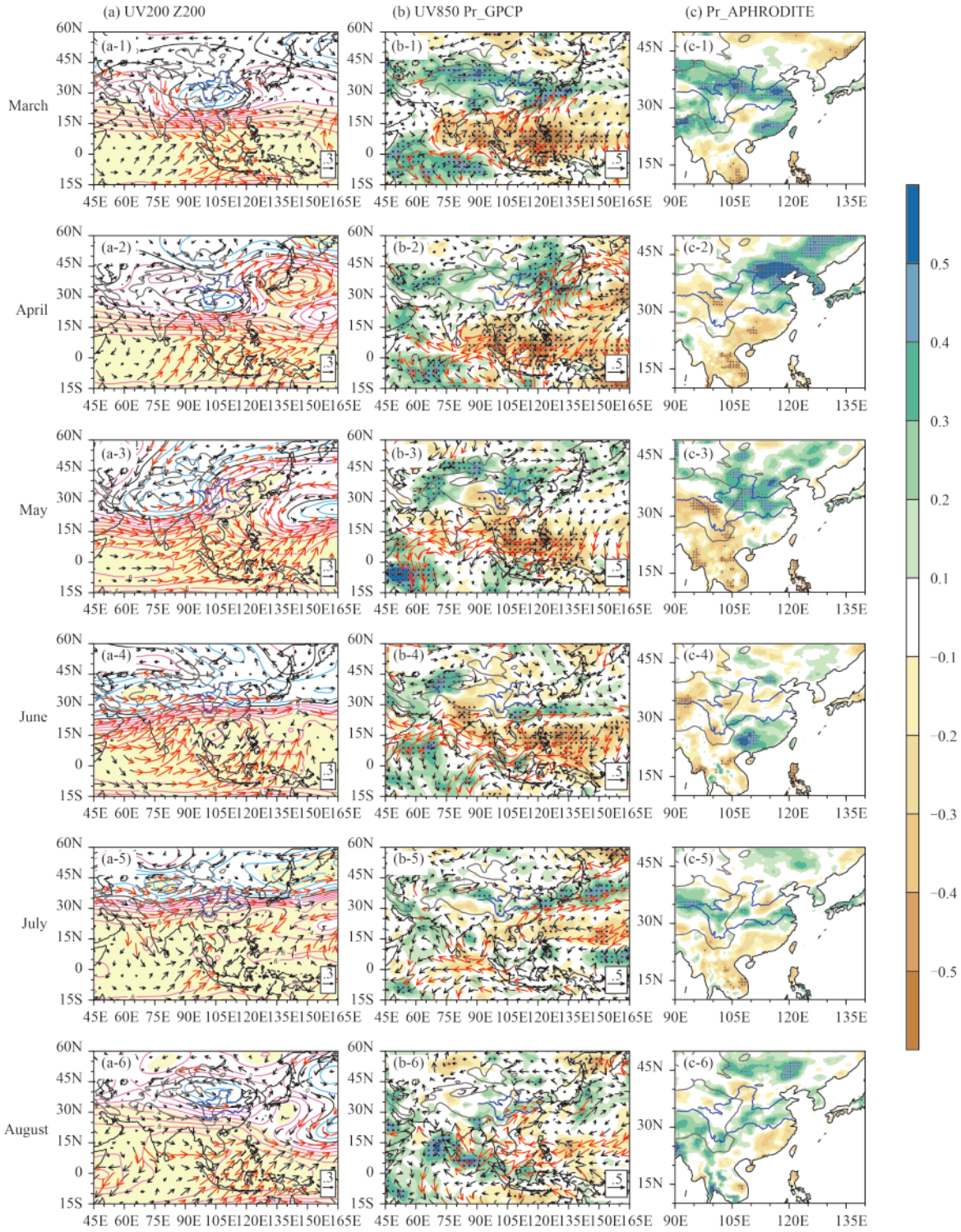

Fig. 3. Simultaneous correlation maps between the IOBM index and the circulation/precipitation from March (top row) to August (bottom row). The geopotential height at 200 hPa (Z200) is depicted by contours with an interval of 0.1 (black contours are zero; pink contours are positive; blue contours are negative; yellow shading indicates the 95% confidence level) and the horizontal wind at 200 hPa (UV200) is depicted by vectors (red vectors pass the 95% confidence level) (left-hand panels); horizontal wind at 850 hPa (UV850) is depicted by vectors (red vectors pass the 95% confidence level) and Global Precipitation Climatology Project precipitation (Pr_GPCP) is depicted by shading (black dots indicates 95% confidence level) (middle panels); and APHRODITE (Asian Precipitation Highly-Resolved Observational Data Integration Towards Evaluation of Water Resource) precipitation (Pr_APHRODITE) is depicted by shading (black dots indicate the 95% confidence level) (right-hand panels). The grey bold lines represent altitude above 1500 m, and the blue bold lines represent the Yangtze River (in the south) and Yellow River (in the north).

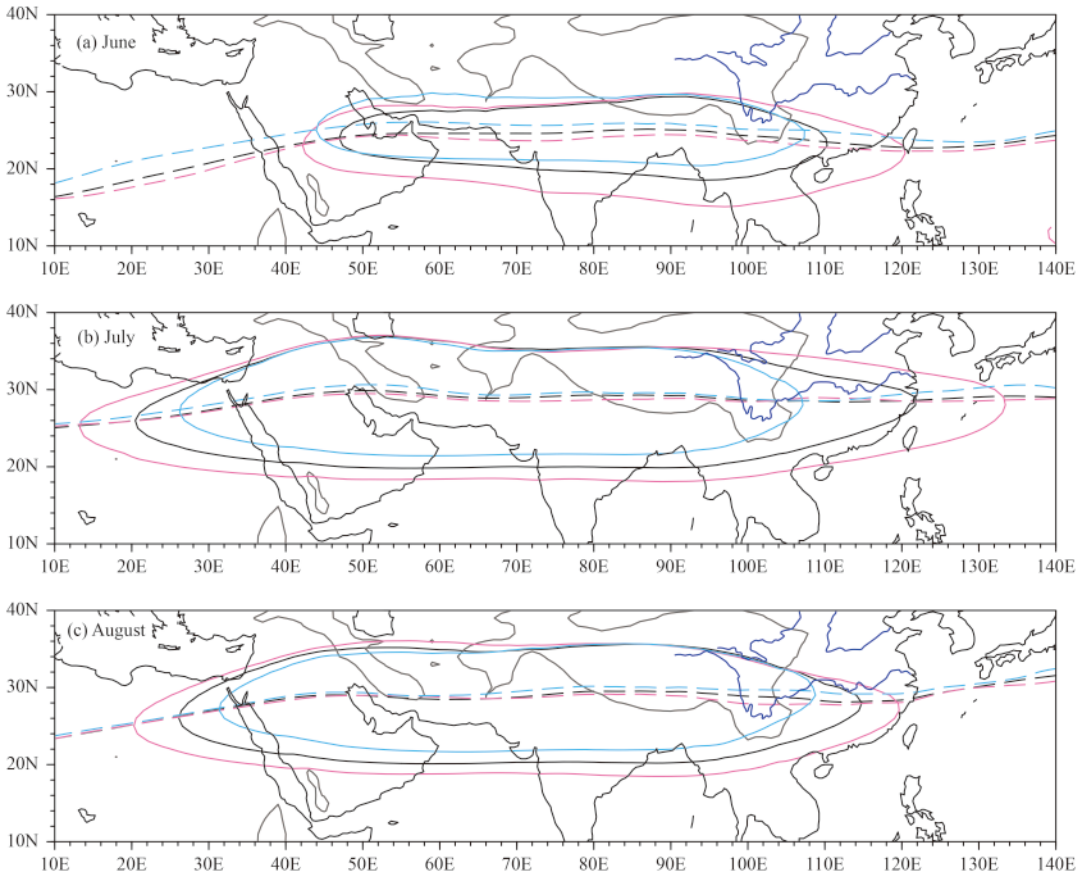

Fig. 4. Coverages of the South Asian high at 200 hPa, depicted by geopotential height (gpm), for (a) June, (b) July, and (c) August. The black contours denote the climatological mean; the red and blue contours denote the composite mean in warm and cold Indian Ocean basin mode years, respectively. Only the contour lines of 12520 are shown for the sake of clarity. The dashed contour is the ridge line of the South Asian high. The grey bold lines represent altitude above 1500 m, and the blue bold lines represent the Yangtze River (in the south) and Yellow River (in the north).

Matsuno–Gill pattern (Matsuno, 1966; Gill, 1980) from March to August (Fig. 3). The anomalous descending branch of the Walker circulation is characterized by an obvious convergence region in the upper troposphere induced by anomalous northwesterly and anomalous southwesterly flow, associated with suppressed convective precipitation. An anomalous easterly prevails at the lower level and expands into the TIO. The anomalous descending branch of the Walker circulation moves eastward obviously, and shifts northward slightly from March to August. Its center is located over Indonesia in March and April, and it migrates from the Philippine Sea to the northwestern Pacific from May to August.

In the lower troposphere, a remarkable anomalous anticyclone persists over the tropical Northwest Pacific from March to August (Fig. 3b). Note that the anomalous anticyclone is closely related to the anomaly of the western North Pacific subtropical high. Composite analysis shows that a warm IOBM promotes the westward advancement of the western North Pacific subtropical high from March to August, while the cold IOBM induces it to retreat eastward (Fig. 5). The ridge line of the western North Pacific subtropical high tends to move equatorward slightly when the IOBM warms in summer. Thus, it varies apparently in the zonal direction but inconspicuously in the meridional direction with the anomalous IOBM.

In the subtropics and midlatitudes, the anomalous circulations linked to the IOBM at 200 hPa possess significant differences from March to August (Fig. 3a). The 200-hPa geopotential height anomaly mainly manifests an inhomogeneous distribution along the zonal direction in spring (March–April–May), but along the meridional direction in summer. In spring, positive–negative–positive wave trains of anomalous geopotential height are distributed over the Asian region from the southwest to the northeast. In March and April, the two positive centers are located over the western Tibetan Plateau and Japan, respectively, accompanied by a negative center located over the southeastern Tibetan Plateau. In May, the two positive centers exist over the Arabian Sea and eastern China, respectively, with the negative center located over

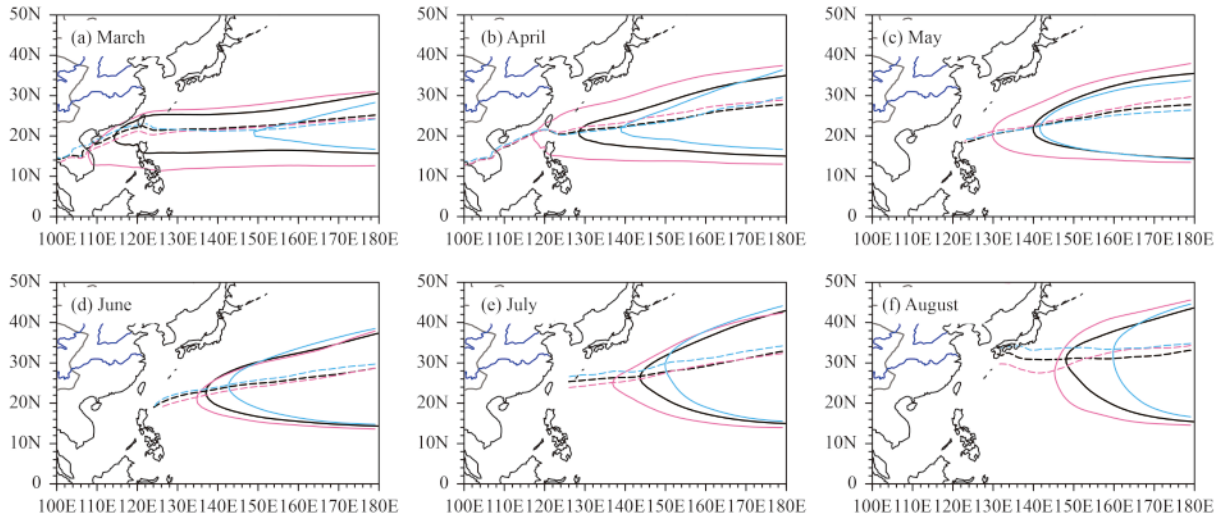

Fig. 5. Coverages of the western North Pacific subtropical high at 850 hPa, depicted by geopotential height (gpm), from (a) March to (f) August. The black contours denote the climatological mean; and the red and blue contours denote the composite mean in warm and cold Indian Ocean basin mode years, respectively. Only the contour lines of 1520 are shown for the sake of clarity. The dashed contour is the ridge line of the western North Pacific subtropical high. The grey bold lines represent altitude above 1500 m, and the blue bold lines represent the Yangtze River (in the south) and Yellow River (in the north).

the mid–western Tibetan Plateau. The anomalous highs to the west of the Tibetan Plateau are the Rossby wave response to the convective condensation heating over the warm TIO. The wave trains result from the energy dispersion of the stationary Rossby wave along the Asian westerly wind jet (Ding and Wang, 2005; Yang et al., 2009; Xie et al., 2009). In June and July, the 200-hPa geopotential height anomaly displays a positive–negative seesaw pattern between the tropical region and the midlatitude region. The zero line resides at 25°N in June and 30°N in July. In August, an anomalous low is situated over the Yellow River valley, with positive anomalous geopotential height surrounding it.

Since the anomalous wind and geopotential height over the subtropical and midlatitude region meet the quasigeostrophic equilibrium, the anomalous wind follows the anomalous geopotential height gradient (Fig. 3a). Therefore, anomalous southerly wind in spring and anomalous westerly wind in June and July prevail over East Asia at 200 hPa. As a result, the upper-level circulations are dominated by an anomalous anticyclone in spring, enhanced westerly flow in June and July, and an anomalous cyclone in August. The different patterns between spring and summer may be attributable to the onset and establishment of the EASM, leading to the prominently enhanced climatological northerly wind over South China and easterly wind on the southern flank of the Tibetan Plateau in the upper troposphere. The basic flow changes impact the maintenance of the stationary Rossby wave. For the East Asian jet, as an important upper-level circulation, the composite analysis shows a warm IOBM is conducive to it slanting and amplifying to the northeast in spring, expanding and intensifying to the east in June and July, but shrinking and weakening in August (Fig. 6). Its ridge line moves southward in summer, which is identical to the result of Qu and Huang (2012).

Over East Asia, the southwest–northeast oriented main rainband (called Meiyu in China, Changma in Korea, and Baiu in Japan) marches northward and brings the rainy season (Ding and Chan, 2005). Dominated by anomalous circulation in the upper and lower troposphere with a warm IOBM, the precipitation anomaly displays quite differently from March to August (Figs. 3b and 3c). In March, there are two obvious positive anomalous rainfall bands. One expands from the northern Tibetan Plateau to southern Japan and the other from the southeastern coast of China to southern Japan. In April, the positive anomalous rainfall covers from northeastern Asia to southern Japan. In May, the rainfall is above-normal over the Yellow River valley. Note that the enhanced precipitation regions in spring, except the southern branch in March, do not overlap with the climatological main rainfall bands, although they pass the 95% confidence level. In spring, the low-level southwesterly associated with the anomalous anticyclone over Northwest Pacific transports more moisture to North China. In addition, the anomalous divergence induced by the anomalous anticyclone over East Asia in the upper layers promotes ascending motion. Such a circulation structure plays an import-

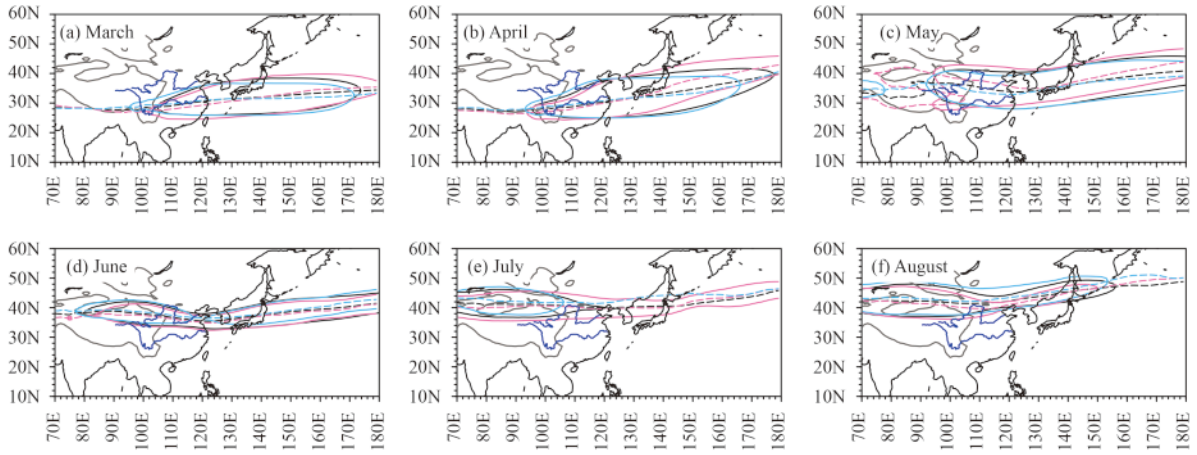

Fig. 6. Locations of the East Asian jet at 200 hPa, depicted by zonal wind (m s^{-1}), from (a) March to (f) August. The black contours denote the climatological mean; and the red and blue contours denote the composite mean in warm and cold Indian Ocean basin mode years, respectively. Only the contour lines of 50 in (a), 38 in (b), 30 in (c, d), 25 in (e, f) are shown for the sake of clarity. The dashed contour is the ridge line of the East Asian jet. The grey bold lines represent altitude above 1500 m, and the blue bold lines represent the Yangtze River (in the south) and Yellow River (in the north).

ant role in the enhanced precipitation in spring. In June, the enhanced rainfall band expands from the southern region of the Yangtze River to the East China Sea. In July, it expands from the Yangtze River to Japan. In August, it is located over the region between the Yangtze River and the Yellow River. It can be clearly seen that the enhanced rainfall band moves from the south to the north in summer, accompanying the northward march of the climatological main rainfall band in summer. Hu and Duan (2015) suggested that the IOBM has no significant impact on precipitation in summer over eastern China, the Korean Peninsula, and Japan. In eastern China, the anomalous precipitation patterns are almost opposite between June and August, and a similar case can be found around Japan between June and July. The opposite contribution from the IOBM can account for the disappearance of the significantly influential region induced by the counteracting effect when calculating the summer mean. In terms of whether the IOBM has a linkage with the march of the northern boundary of the East Asian rainfall band, the composite analysis shows that the 4-mm day^{-1} contours of the precipitation rate derived from the climatology and warm/cold IOBM events nearly overlap (Fig. 7). It seems that the IOBM does not alter the marching process apparently, but only modifies the intensity of the East Asian main rainfall band. To a greater extent, the displacement of the rainfall band depends on the meridional position of the South Asian high, the East Asian jet, and the western North Pacific subtropical high. The results mentioned above imply that their ridge lines do not vary greatly in meridional displacement when forced by the IOBM.

3.3 *Sub-seasonal relationship between East Asian climate and the IODM*

For the IODM, the simultaneous correlation maps show that the relationships between the IODM and the circulation/precipitation over East Asia are rather weak from spring to summer (Fig. 8). Under the condition of a positive phase of the IODM, in March, the positive precipitation anomalies tend to appear over Northeast Asia and the Indochina Peninsula. In April, the enhanced precipitation is located over the Indochina Peninsula and South China, while the suppressed precipitation is located over North China. In May, the suppressed precipitation and the associated anomalous low-level northwesterly reside over East China. In June, South China and downstream of the Yellow River tend to be wet, while the regions from northeastern Asia to Japan tend to be dry. In July, the precipitation is above-normal over North China and the southern coast of China. The suppressed rainfall associated with an anomalous anticyclone covers southern Japan. In August, the positive anomaly of precipitation occurs over the Indochina Peninsula and southwestern China. Overall, the significant wind anomalies at the upper and lower levels cover few regions, implying that the IODM plays an unimportant role in the circulation anomaly over East Asia during spring and summer, which is consistent with the results of Yang et al. (2010).

4. Circulation and precipitation responses to the TIO SST in an AGCM

4.1 *Model and experiment design*

The AGCM used in the present study, i.e., FAMIL,

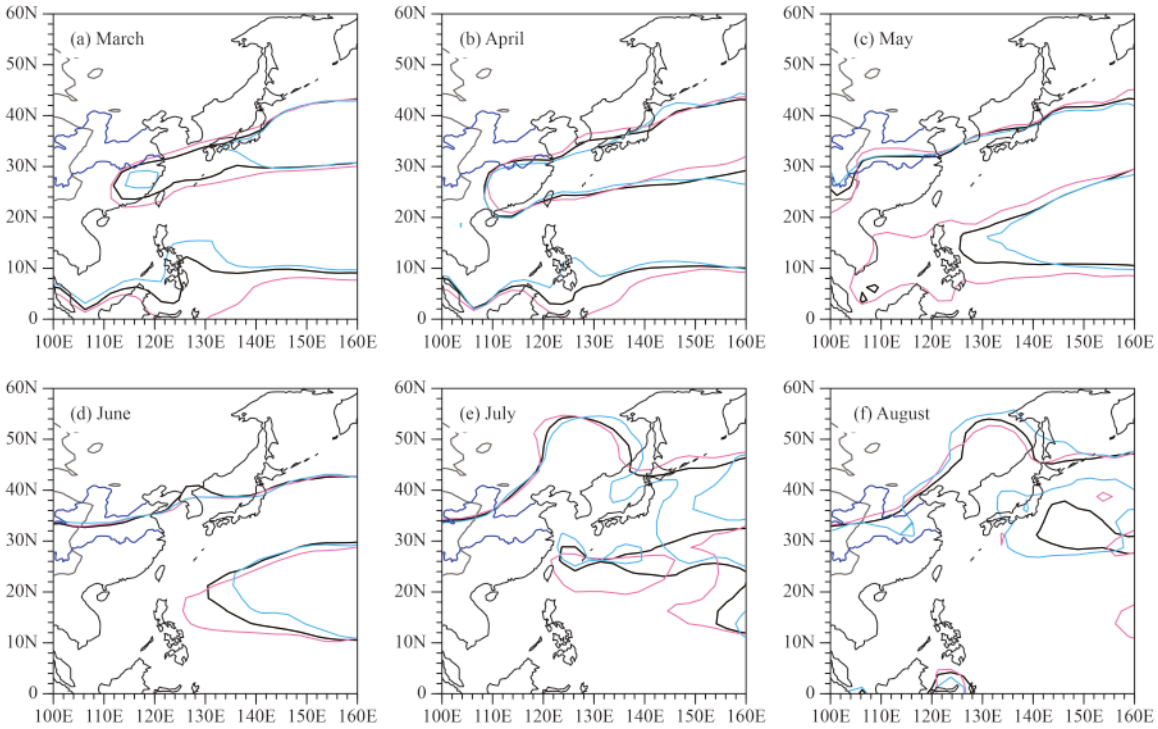

Fig. 7. The main rainfall belts depicted by the 4-mm day^{-1} precipitation rate from (a) March to (f) August. The black contours denote the climatological mean; and the red and blue contours denote the composite mean in warm and cold IOBM years, respectively. The grey bold lines represent altitude above 1500 m, and the blue bold lines represent the Yangtze River (in the south) and Yellow River (in the north).

has a reasonable capacity to simulate the Asian climate in the annual periodic climatology, the interannual variability, and the seasonal march, so it has been widely used in researching the climatic dynamics of the Asian monsoon, the tropical ocean, and the Tibetan Plateau (Liu et al., 2004; Wu et al., 2012; Duan et al., 2013; Hu and Duan, 2015). The climate mean low-level circulation and precipitation from March to August shows an overall similarity between the observation and the FAMIL control experiment (Fig. 9). FAMIL can reproduce the dominant systems over the TIO and the Asian region well, i.e., the Somali jet, the monsoon trough, the western North Pacific subtropical high, the southwesterly over southern China, and the East Asian main rainfall belt. The deficiency of the model can be summarized as the overestimated precipitation over the TIO, the western Pacific, and the Tibetan Plateau region, whereas the precipitation over the east coast of the Bay of Bengal and the East Asian subtropical region is underestimated. Meanwhile, the East Asian main rainfall belt shifts more northward in comparison with the observations, which might be related to the amplification and the westward expansion of the western North Pacific subtropical high.

To verify the conclusions derived from the observed analysis and further study the impacts of the TIO SST anomaly on the East Asian climate in the model simulation, a series of AGCM simulation experiments are performed. Table 3 shows the design of the AGCM numerical simulation experiments. The AMIP2 experiment is performed to estimate the standard variances of the circulation and precipitation in simulation results. The control experiment (CTL) is performed for the evaluation of the model as mentioned above (Fig. 9). Note that the SST anomalies in the sensitivity experiments (IOBM-POS, IOBM-NEG, IODM-POS, and IODM-NEG) are only implemented in the TIO (30°S–30°N, 30°–105°E) from March to August, whereas the climatological monthly SST is given in the other regions and months, the same as in the control run. The intensity of the SST anomaly is 2.5 times the standard deviation of the natural interannual variability. A 25-point spatial running average is applied to the SST anomaly at the boundary of the TIO to smooth the discontinuous gradient. The integration length of the experiments is listed in Table 3, which does not include the one year used in advance for spin-up.

4.2 *Circulation and precipitation responses to the IOBM and IODM*

In the experiments with the forcing of the IOBM, the response shows overall similar spatial patterns of circulation and precipitation as observed from March to August (Fig. 10). The warm phase of the IOBM can successfully

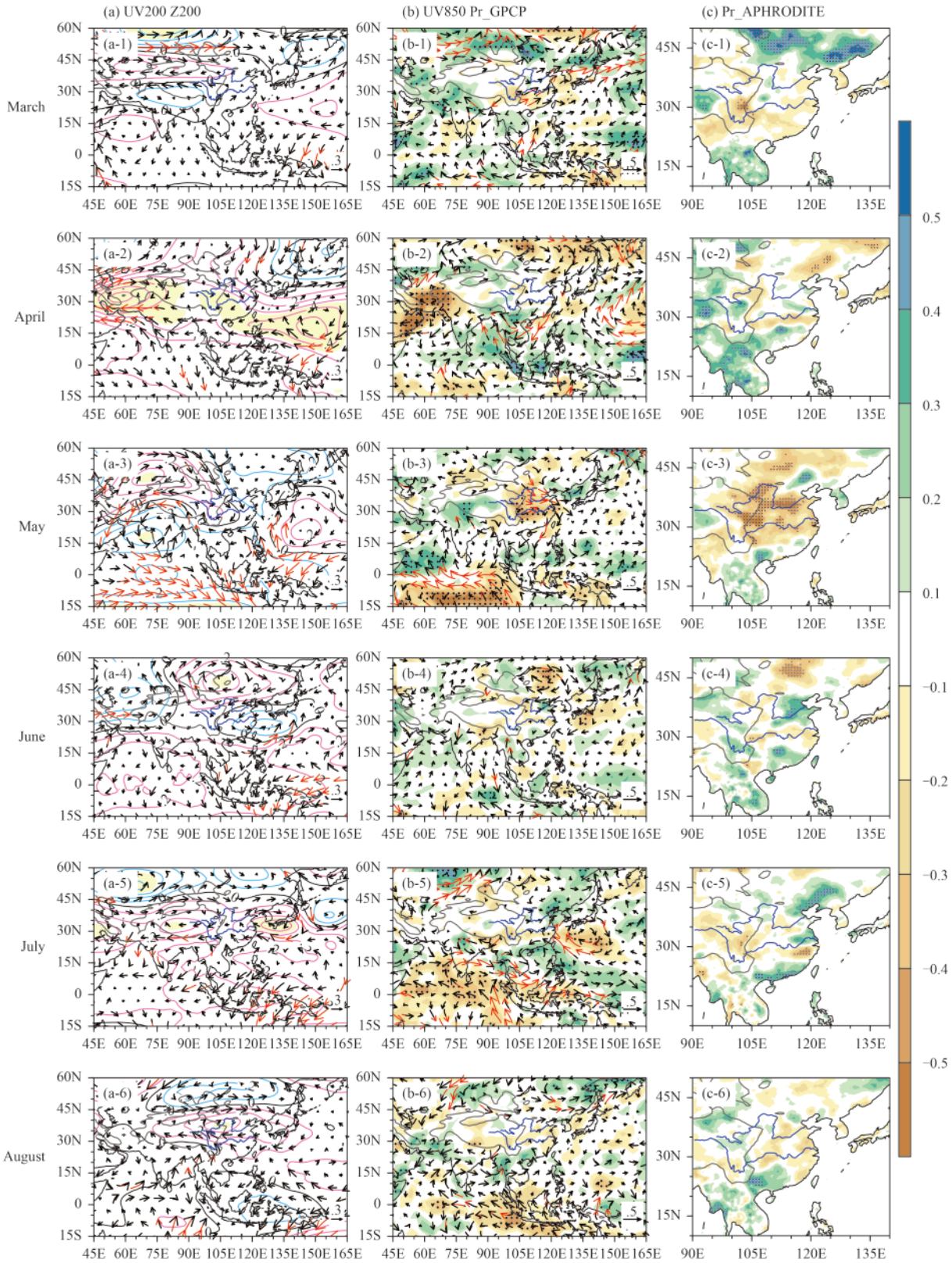

Fig. 8. As in Fig. 3, but for the IODM index.

reproduce the Matsuno–Gill pattern response (Matsuno, 1966; Gill, 1980) over the TIO from March to August. At 200 hPa, the significant positive geopotential height occurs from the TIO to the western Pacific. Under the con-

Table 3. Design of the AGCM numerical simulation experiments

Experiment	Design	Integration length (yr)
AMIP2	Global SSTa ice prescribed by AMIP2 from 1979 to 2009	31
CTL	Annual periodic climatological monthly SSTa ice	20
IOBM-POS	Adding positive EOF1 anomaly of SST in the TIO	20
IOBM-NEG	Adding negative EOF1 anomaly of SST in the TIO	20
IODM-POS	Adding positive EOF2 anomaly of SST in the TIO	20
IODM-NEG	Adding negative EOF2 anomaly of SST in the TIO	20

dition of static equilibrium in the vertical direction, the 200-hPa geopotential height anomaly is proportional to the temperature integration from the surface to 200 hPa. The warm SST increases the tropospheric temperature through the moist adiabatic adjustment in deep convection (Xie et al., 2009; Qu and Huang, 2012). This explains why the warm SST can elevate the geopotential height. Consequently, the south of the South Asian high evidently strengthens in summer. A striking high tongue wedges into the western Pacific, which is induced by the eastward propagating Kelvin wave, leading to a westward-expanded western North Pacific subtropical high. Another high is located on the northwestern side of the TIO, which is induced by the westward propagating Rossby wave (Xie et al., 2009). Concurrently, a convergence of northwesterly and southwesterly wind in the upper troposphere is situated over the Maritime Continent and an anomalous easterly prevails in the lower troposphere. The circulation response patterns from the TIO to the western Pacific in the numerical simulations are quite similar to the observed results. The model reproduces the anomalous anticyclone over the tropical Northwest Pacific, which persists from March to August. The eastward propagating Kelvin intensifies the anomalous anticyclone via the Ekman divergence mechanism (Xie et al., 2009). Synchronously, the associated easterly anomaly on the southern flank of the anomalous anticyclone results in the warming of the North Indian Ocean and the South China Sea. Such an inter-basin coupled positive feedback supports the persistence of the anomalous anticyclone (Kosaka et al., 2013). In fact, the anomalous anticyclone and the westward-expanded western North Pacific subtropical high are the tropical lobes of the PJ or EAP pattern, which intensify the low-level southwesterly flow over South China. The suppressed precipitation over the tropical Northwest Pacific triggers the tropical-extratropical teleconnection of the PJ or EAP pattern, significantly impacting the climate anomaly over East Asia (Nitta, 1987; Huang and Sun, 1992; Lau et al., 2000; Wang et al., 2001; Kim et al., 2009). For the upper circulation in the subtropics and midlatitudes, the IOBM is able to excite a positive–negative–positive wave train expanding from northeastern Africa to northeastern Asia in spring. The anomalous low associated with the anomalous anticyclone is reproduced well over China in August. However, the zonally distributed anomalous low is not present in the midlatitudes in June and July, possibly due to model deficiency, so the downstream East Asian jet cannot be supported to significantly intensify, which renders the anomalous westerly weaker than that in the observations over East Asia. Furthermore, the precipitation anomaly patterns are overall consistent with the observed results. However, the positive anomalous precipitation regions tend to move northward in summer in the model simulation, which may again be attributable to model bias.

The simulated response forced by the IODM (Fig. 11) also shows overall similar precipitation anomaly patterns over East Asia as in the observations; however, the wind anomalies at the upper and lower level are still largely insignificant. This confirms that the IODM forcing has little impact on East Asian climate during spring and summer.

The above results from the analysis of observation and model simulations indicate that the anomalous response of circulation and precipitation to the IOBM and IODM vary remarkably from March to August, possibly due to the drastic climatological mean flow changes. The climatic state evolves a distinguishable change from March to August. From May, the Asian monsoon arises with the establishment of the southwesterly monsoon over the North Indian Ocean and the enhancement of southwesterly wind over South China. Synchronously, easterly wind replaces westerly wind at the southern flank of the Tibetan Plateau in the upper troposphere (Ding and Chan, 2005).

5. Conclusions

The present paper, based on multi-source observational data from 1979 to 2013, investigates the relationship between the TIO SST anomaly and the sub-seasonal evolution of the circulation and rainfall over East Asia during boreal spring and summer using correlation analysis and composite analysis. The results from a series of numerical simulations using an AGCM are also used to explain the diagnosis results. The main conclusions can be summarized as follows.

The two leading modes of the interannual variability

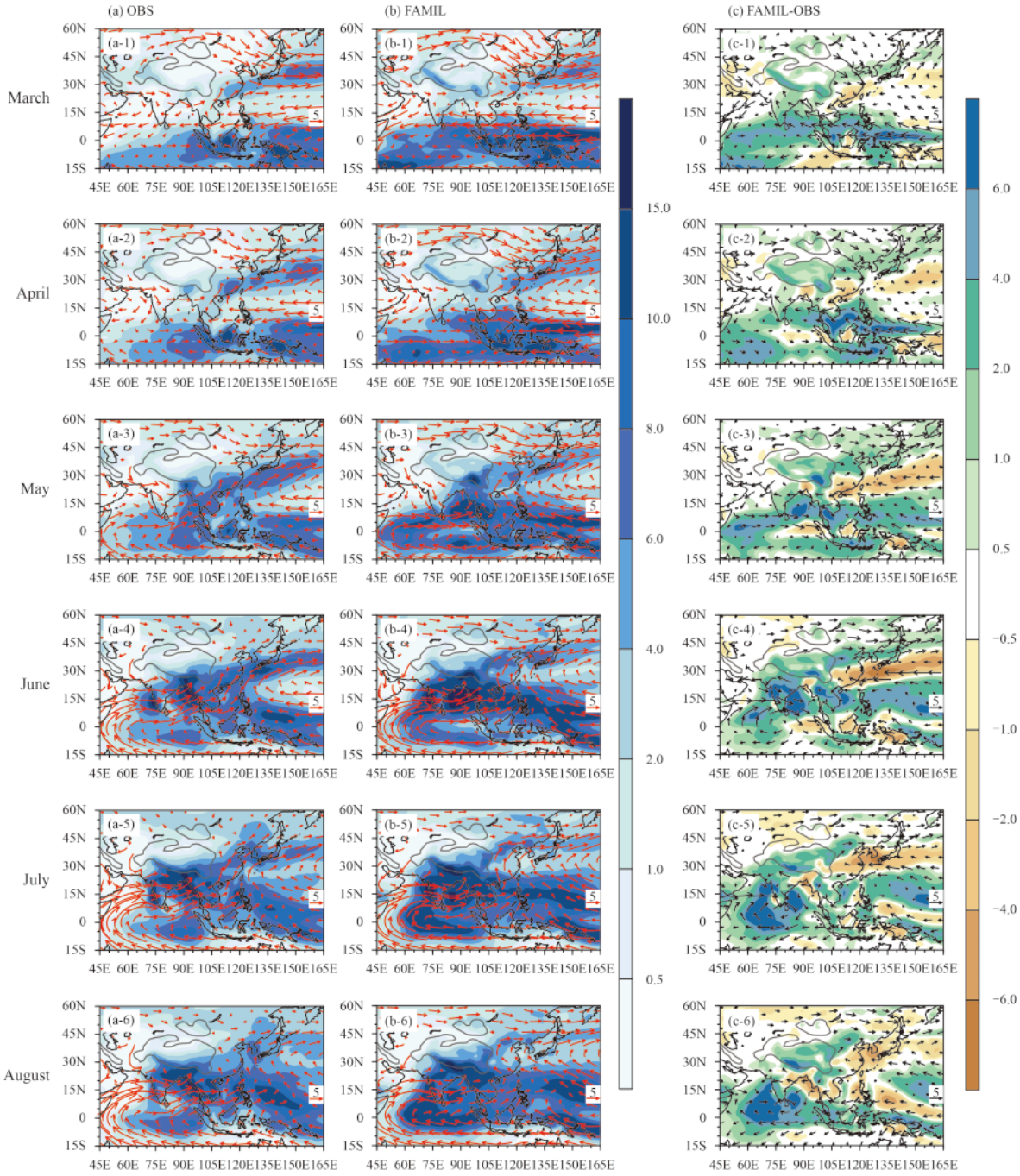

Fig. 9. Climate mean 850-hPa horizontal wind (vectors; m s^{-1}) and precipitation (color shading; mm day^{-1}) from March (top row) to August (bottom row) in observations (left-hand panels), the control run of FAMIL (Finite-volume Atmospheric Model developed by IAP/LASG) (middle panels), and their difference fields (right-hand panels). The grey bold lines represent altitude above 1500 m.

of the TIO SST anomaly, i.e., the IOBM and IODM, account for around 50% of the explained variance. The persistence of the IOBM is relatively stronger than that of the IODM. The remote forcing of the IOBM can significantly impact the sub-seasonal evolution of the circulation and rainfall over East Asia, primarily attributable to two paths. Firstly, in the lower troposphere, a warm IOBM induces an anomalous anticyclone and suppressed precipitation over the tropical Northwest Pacific via an eastward propagating Kelvin wave, which enhances the southwesterly flow over South China and triggers the PJ/EAP teleconnection pattern from March to August. Secondly, in the upper troposphere, a warm IOBM excites a positive–negative–positive wave train of anomalous geopotential height over the Asian region in spring, displays a positive–negative seesaw pattern

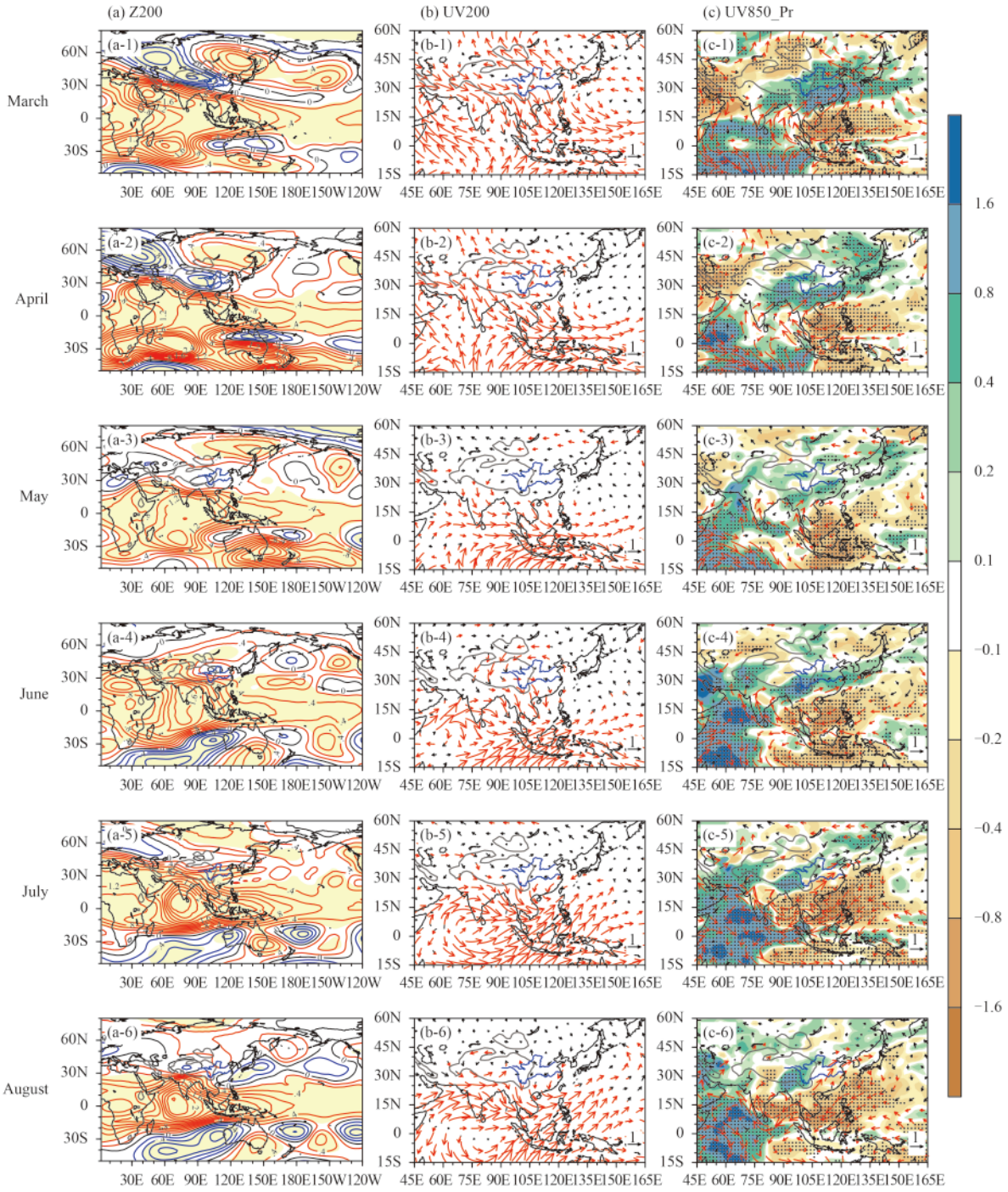

Fig. 10. Normalized difference fields of circulation and precipitation from March (top row) to August (bottom row) derived from the Indian Ocean basin mode forcing experiments. The difference between the positive and negative anomaly sensitivity experiments is divided by the standard deviation estimated by the AMIP2 forcing experiments, which is defined as the normalized difference fields. The 200-hPa geopotential height (Z200) is depicted by contours with intervals of 0.2 (black contours are zero; red contours are positive; blue contours are negative; yellow shading indicates the 95% confidence level) (left-hand panels); the 200-hPa wind (UV200) is depicted by vectors (red vectors pass the 95% confidence level) (middle panels); and the 850-hPa wind (UV850) is depicted by vectors (red vectors pass the 95% confidence level) and the precipitation (Pr) is depicted by shading (black dots indicate the 95% confidence level) (right-hand panels). The grey bold lines represent altitude above 1500 m, and the blue bold lines represent the Yangtze River (in the south) and Yellow River (in the north).

between the tropics and midlatitudes in June and July, and generates an anomalous low over the Yellow River valley in August. The geopotential height anomaly results in an anomalous anticyclone in spring over the eastern coast of East Asia, an enhanced subtropical westerly jet over East Asia in June and July, and an anomalous

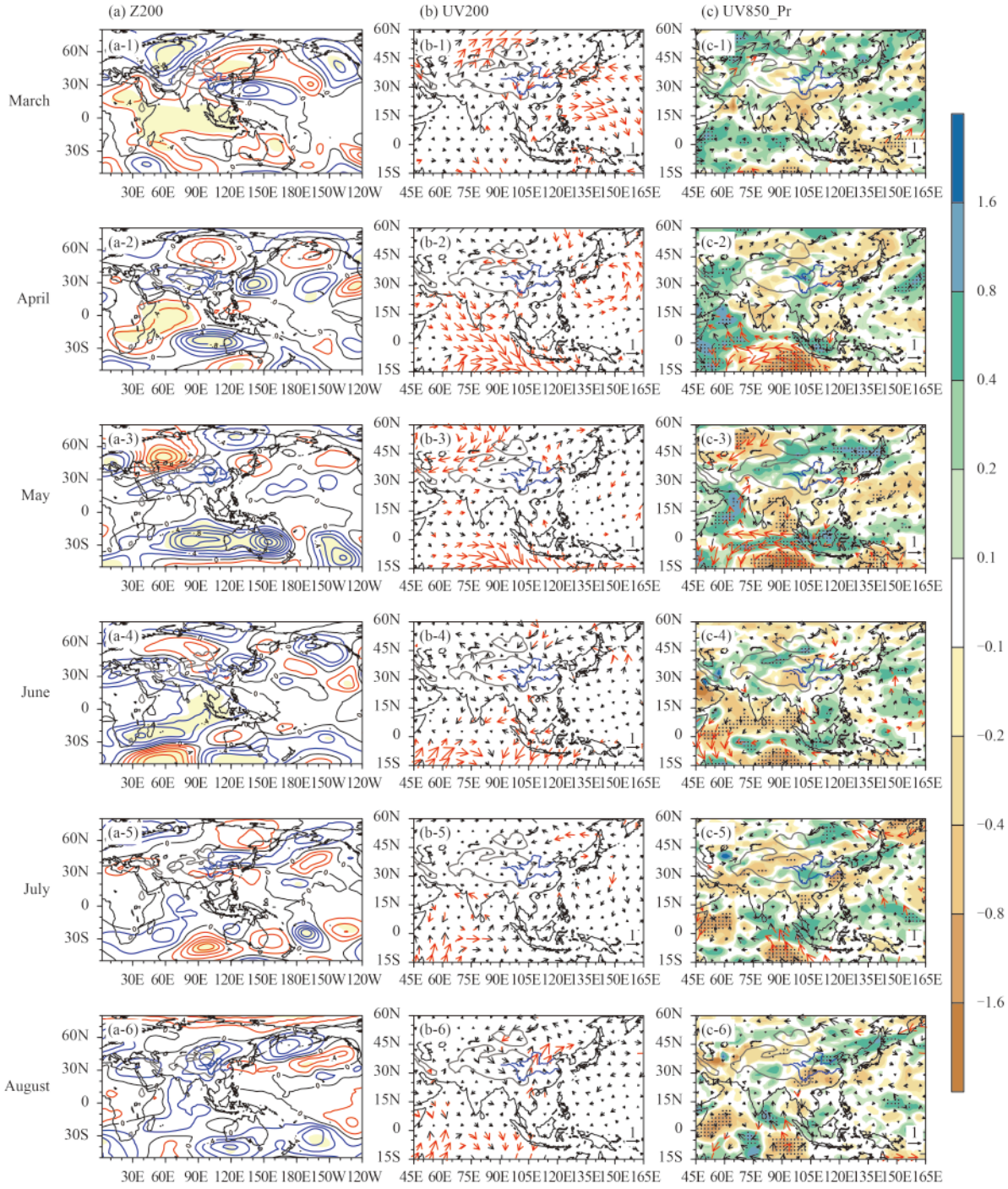

Fig. 11. As in Fig. 10, but derived from the IODM forcing experiments.

cyclone over the Yellow River valley in August. Besides, a warm IOBM induces a westward-expanded northwestern Pacific subtropical high in spring and summer and an enhanced South Asian high in summer. The East Asian jet expands to the northeast in spring, strengthens to the east in June and July, but shrinks in August. These circulation systems collectively modulate the evolution of the precipitation anomaly over East Asia. In March, two enhanced rainfall bands expand from the northern Tibetan Plateau to southern Japan and from the southeastern coast of China to southern Japan, respectively. The positive anomalous rainfall covers from northeastern Asia to southern Japan in April, and the rainfall is above-normal over the Yellow River valley in May. In summer, the IOBM only strengthens the northward-marching main rainfall band rather than alters the marching process. The

enhanced rainfall bands expand from the southern region of the Yangtze River to the East China Sea in June, cover from the Yangtze River to Japan in July, and exist over the region between the Yangtze River and the Yellow River in August. However, the IODM has a much weaker effect on the climate anomaly over East Asia during spring and summer. The impacts of the TIO SST anomaly on the circulation and rainfall over East Asia vary remarkably from spring to summer. These results are also verified by numerical simulations based on an AGCM.

The present paper focuses on the atmospheric response forced by the TIO SST anomaly and employs the results of AGCM simulations to confirm the findings. In the future work, the impacts of the TIO SST anomaly on the climatic anomaly in East Asia should be discussed in a land–air–sea coupled framework. Besides, how the SST anomalies in other ocean regions impact upon the subseasonal evolution of the circulation and rainfall in East Asia should also be taken into account.

Acknowledgments. The authors are grateful to Jun Hu for his assistance in using the AGCM.

REFERENCES

Adler, R. F., G. J. Huffman, A. Chang, et al., 2003: The version-2 Global Precipitation Climatology Project (GPCP) monthly precipitation analysis (1979–present). *Journal of Hydrometeorology*, **4**, 1147–1167, doi:10.1175/1525-7541(2003)004<1147:TVGPCP>2.0.CO;2.

Chowdary, J. S., S.-P. Xie, J.-J. Luo, et al., 2011: Predictability of Northwest Pacific climate during summer and the role of the tropical Indian Ocean. *Climate Dyn.*, **36**, 607–621, doi: 10.1007/s00382-009-0686-5.

Dee, D. P., S. M. Uppala, A. J. Simmons, et al., 2011: The ERA-Interim reanalysis: Configuration and performance of the data assimilation system. *Quart. J. Roy. Meteor. Soc.*, **137**, 553–597, doi: 10.1002/qj.828.

Ding, Q. H., and B. Wang, 2005: Circumglobal teleconnection in the Northern Hemisphere summer. *J. Climate*, **18**, 3483–3505, doi: 10.1175/JCLI3473.1.

Ding, Y. H., and J. C. L. Chan, 2005: The East Asian summer monsoon: An overview. *Meteor. Atmos. Phys.*, **89**, 117–142, doi: 10.1007/s00703-005-0125-z.

Du, Y., S. P. Xie, G. Huang, et al., 2009: Role of air–sea interaction in the long persistence of El Niño-induced North Indian Ocean warming. *J. Climate*, **22**, 2023–2038, doi: 10.1175/2008JCLI2590.1.

Duan, A. M., M. R. Wang, Y. H. Lei, et al., 2013: Trends in summer rainfall over China associated with the Tibetan Plateau sensible heat source during 1980–2008. *J. Climate*, **26**, 261–275, doi: 10.1175/JCLI-D-11-00669.1.

Gill, A. E., 1980: Some simple solutions for heat-induced tropical circulation. *Quart. J. Roy. Meteor. Soc.*, **106**, 447–462.

Guan, Z. Y., and T. Yamagata, 2003: The unusual summer of 1994 in East Asia: IOD teleconnections. *Geophys. Res. Lett.*, **30**, 1544, doi: 10.1029/2002GL016831.

Guan, Z. Y., K. Ashok, and T. Yamagata, 2003: Summertime response of the tropical atmosphere to the Indian Ocean dipole sea surface temperature anomalies. *J. Meteor. Soc. Japan*, **81**, 531–561.

He, C., T. J. Zhou, and B. Wu, 2015: The key oceanic regions responsible for the interannual variability of the western North Pacific subtropical high and associated mechanisms. *J. Meteor. Res.*, **29**, 562–575, doi: 10.1007/s13351-015-5037-3.

Hu, J., and A. M. Duan, 2015: Relative contributions of the Tibetan Plateau thermal forcing and the Indian Ocean sea surface temperature basin mode to the interannual variability of the East Asian summer monsoon. *Climate Dyn.*, **45**, 2697–2711, doi: 10.1007/s00382-015-2503-7.

Huang, G., K. M. Hu, and S. P. Xie, 2010: Strengthening of tropical Indian Ocean teleconnection to the Northwest Pacific since the mid-1970s: An atmospheric GCM Study. *J. Climate*, **23**, 5294–5304.

Huang, R. H., and F. Y. Sun, 1992: Impacts of the tropical western Pacific on the East Asian summer monsoon. *J. Meteor. Soc. Japan*, **70**, 243–256.

Kim, J.-E., S.-W. Yeh, and S.-Y. Hong, 2009: Two types of strong Northeast Asian summer monsoon. *J. Climate*, **22**, 4406–4417, doi: 10.1175/2009JCLI2434.1.

Klein, S. A., B. J. Soden, and N. C. Lau, 1999: Remote sea surface temperature variations during ENSO: Evidence for a tropical atmospheric bridge. *J. Climate*, **12**, 917–932.

Kosaka, Y., S. P. Xie, N. C. Lau, et al., 2013: Origin of seasonal predictability for summer climate over the northwestern Pacific. *Proc. Natl. Acad. Sci. U. S. A.*, **110**, 7574–7579, doi: 10.1073/pnas.1215582110.

Lau, K.-M., K.-M. Kim, and S. Yang, 2000: Dynamical and boundary forcing characteristics of regional components of the Asian summer monsoon. *J. Climate*, **13**, 2461–2482, doi: 10.1175/1520-0442(2000)013<2461:DABFCO>2.0.CO;2.

Li, C. Y., and M. Q. Mu, 2001: The influence of the Indian Ocean dipole on atmospheric circulation and climate. *Adv. Atmos. Sci.*, **18**, 831–843. (in Chinese)

Li, S. L., J. Lu, G. Huang, et al., 2008: Tropical Indian Ocean basin warming and East Asian summer monsoon: A multiple AGCM study. *J. Climate*, **21**, 6080–6088, doi: 10.1175/2008JCLI2433.1.

Li, T., Y. S. Zhang, C.-P. Chang, et al., 2001: On the relationship between Indian Ocean sea surface temperature and Asian summer monsoon. *Geophys. Res. Lett.*, **28**, 2843–2846, doi: 10.1029/2000GL011847.

Liu, Y. M., G. X. Wu, and R. C. Ren, 2004: Relationship between the subtropical anticyclone and diabatic heating. *J. Climate*, **17**, 682–698, doi: 10.1175/1520-0442(2004)017<0682:RBTSAA>2.0.CO;2.

Lu, R. Y., and S. Lu, 2015: Asymmetric relationship between Indian Ocean SST and the western North Pacific summer monsoon. *J. Climate*, **28**, 1383–1395, doi: 10.1175/JCLI-D-14-00289.1.

Matsuno, T., 1966: Quasi-geostrophic motions in the equatorial area. *J. Meteor. Soc. Japan*, **44**, 25–43.

Nitta, T., 1987: Convective activities in the tropical western Pacific and their impact on the Northern Hemisphere summer circulation. *J. Meteor. Soc. Japan*, **65**, 373–390.

Qu, X., and G. Huang, 2012: Impacts of tropical Indian Ocean SST on the meridional displacement of East Asian jet in boreal summer. *Int. J. Climatol.*, **32**, 2073–2080, doi: 10.1002/joc.2378.

Rayner, N. A., D. E. Parker, E. B. Horton, et al., 2003: Global analyses of sea surface temperature, sea ice, and night marine air temperature since the late nineteenth century. *J. Geophys. Res.*, **108**, 4407, doi: 10.1029/2002JD002670.

Saji, N. H., and T. Yamagata, 2003: Possible impacts of Indian Ocean dipole mode events on global climate. *Climate Research*, **25**, 151–169, doi: 10.3354/cr025151.

Saji, N. H., B. N. Goswami, P. N. Vinayachandran, et al., 1999: A dipole mode in the tropical Indian Ocean. *Nature*, **401**, 360–363, doi: 10.1038/43855.

Terao, T., and T. Kubota, 2005: East–west SST contrast over the tropical oceans and the post El Niño western North Pacific summer monsoon. *Geophys. Res. Lett.*, **32**, L15706, doi: 10.1029/2005GL023010.

Wang, B., R. G. Wu, and K.-M. Lau, 2001: Interannual variability of the Asian summer monsoon: Contrasts between the Indian and the western North Pacific–East Asian monsoons. *J. Climate*, **14**, 4073–4090, doi: 10.1175/1520-0442(2001)014<4073:IVOTAS>2.0.CO;2.

Wang, B., Z. W. Wu, J. P. Li, et al., 2008: How to measure the strength of the East Asian summer monsoon. *J. Climate*, **21**, 4449–4463, doi: 10.1175/2008JCLI2183.1.

Webster, P. J., A. M. Moore, J. P. Loschnigg, et al., 1999: Coupled ocean–atmosphere dynamics in the Indian Ocean during 1997–98. *Nature*, **401**, 356–360, doi: 10.1038/43848.

Wu, B., T. Li, and T. J. Zhou, 2010: Relative contributions of the Indian Ocean and local SST anomalies to the maintenance of the western North Pacific anomalous anticyclone during the El Niño decaying summer. *J. Climate*, **23**, 2974–2986, doi: 10.1175/2010JCLI3300.1.

Wu, B., T. J. Zhou, and T. Li, 2009: Seasonally evolving dominant interannual variability modes of East Asian climate. *J. Climate*, **22**, 2992–3005, doi: 10.1175/2008JCLI2710.1.

Wu, G. X., and H. Z. Liu, 1995: Neighborhood response of rainfall to tropical sea surface temperature anomalies. Part I: Numerical experiment. *Chinese J. Atmos. Sci.*, **19**, 422–434. (in Chinese)

Wu, G. X., P. Liu, Y. M. Liu, et al., 2000: Impacts of the sea surface temperature anomaly in the Indian ocean on the subtropical anticyclone over the western pacific—Two-stage thermal adaptation in the atmosphere. *Acta Meteor. Sinica*, **58**, 513–522. (in Chinese)

Wu, G. X., Y. M. Liu, B. He, et al., 2012: Thermal controls on the Asian summer monsoon. *Scientific Reports*, **2**, 204, doi: 10.1038/srep00404.

Xie, S. P., K. M. Hu, J. Hafner, et al., 2009: Indian Ocean capacitor effect on Indo–western Pacific climate during the summer following El Niño. *J. Climate*, **22**, 730–747, doi: 10.1175/2008JCLI2544.1.

Xie, S. P., Y. Kosaka, Y. Du, et al., 2016: Indo–western Pacific Ocean capacitor and coherent climate anomalies in post-ENSO summer: A review. *Adv. Atmos. Sci.*, **33**, 411–432, doi: 10.1007/s00376-015-5192-6.

Yang, J. L., and Q. Y. Liu, 2008: The "charge/discharge" roles of the basin-wide mode of the Indian Ocean SST anomaly-influence on the South Asian high in summer. *Acta Oceanologica Sinica*, **30**, 12–19. (in Chinese)

Yang, J. L., Q. Y. Liu, S. P. Xie, et al., 2007: Impact of the Indian Ocean SST basin mode on the Asian summer monsoon. *Geophys. Res. Lett.*, **34**, L02708, doi: 10.1029/2006GL028571.

Yang, J. L., Q. Y. Liu, Z. Y. Liu, et al., 2009: Basin mode of Indian Ocean sea surface temperature and Northern Hemisphere circumglobal teleconnection. *Geophys. Res. Lett.*, **36**, L19705, doi: 10.1029/2009GL039559.

Yang, J. L., Q. Y. Liu, and Z. Y. Liu, 2010: Linking observations of the Asian monsoon to the Indian Ocean SST: Possible roles of Indian Ocean basin mode and dipole mode. *J. Climate*, **23**, 5889–5902, doi: 10.1175/2010JCLI2962.1.

Yang, Y., S.-P. Xie, L. X. Wu, et al., 2015: Seasonality and predictability of the Indian Ocean dipole mode: ENSO forcing and internal variability. *J. Climate*, **28**, 8021–8036, doi: 10.1175/JCLI-D-15-0078.1.

Yatagai, A., O. Arakawa, K. Kamiguchi, et al., 2009: A 44-year daily gridded precipitation dataset for Asia based on a dense network of rain gauges. *SOLA*, **5**, 137–140, doi: 10.2151/sola.2009-035.

Yu, H. Y., Q. Bao, L. J. Zhou, et al., 2014: Sensitivity of precipitation in aqua-planet experiments with an AGCM. *Atmos. Oceanic Sci. Lett.*, **7**, 1–6, doi: 10.3878/j.issn.1674-2834.13.0033.

Yuan, Y., H. Yang, W. Zhou, et al., 2008: Influences of the Indian Ocean dipole on the Asian summer monsoon in the following year. *Int. J. Climatol.*, **28**, 1849–1859, doi: 10.1002/joc.1678.

Zhou, L. J., Y. M. Liu, Q. Bao, et al., 2012: Computational performance of the high-resolution atmospheric model FAMIL. *Atmos. Oceanic Sci. Lett.*, **5**, 355–359.

Zhou, L. J., Q. Bao, Y. M. Liu, et al., 2015: Global energy and water balance: Characteristics from finite-volume atmospheric model of the IAP/LASG (FAMIL1). *Journal of Advances in Modeling Earth Systems*, **7**, 1–20, doi: 10.1002/2014MS000349.

Zhu, Z. W., T. Li, and J. H. He, 2014: Out-of-phase relationship between boreal spring and summer decadal rainfall changes in southern China. *J. Climate*, **27**, 1083–1099, doi: 10.1175/JCLI-D-13-00180.1.

Tech & Copy Editor: Zhirong CHEN
Language Editor: Colin Smith